

# Treating Point Cloud as Moving Camera Videos: A No-Reference Quality Assessment Metric

Zicheng Zhang, Wei Sun, Xiongkuo Min, *Member, IEEE*,  
Yu Fan, and Guangtao Zhai, *Senior Member, IEEE*

**Abstract**—Point cloud is one of the most widely used digital representation formats for 3D contents, the visual quality of which may suffer from noise and geometric shift during the production procedure as well as compression and downsampling during the transmission process. To tackle the challenge of point cloud quality assessment (PCQA), many PCQA methods have been proposed to evaluate the visual quality levels of point clouds by assessing the rendered static 2D projections. Although such projection-based PCQA methods achieve competitive performance with the assistance of mature image quality assessment (IQA) methods, they neglect the dynamic quality-aware information, which does not fully match the fact that observers tend to perceive the point clouds through both static and dynamic views. Therefore, in this paper, we treat the point clouds as moving camera videos and explore the way of dealing with PCQA tasks via using video quality assessment (VQA) methods in a no-reference (NR) manner. First, we generate the captured videos by rotating the camera around the point clouds through four circular pathways. Then we extract both spatial and temporal quality-aware features from the selected key frames and the video clips by using trainable 2D-CNN and pre-trained 3D-CNN models respectively. Finally, the visual quality of point clouds is represented by the regressed video quality values. The experimental results reveal that the proposed method is effective for predicting the visual quality levels of the point clouds and even competitive with full-reference (FR) PCQA methods. The ablation studies further verify the rationality of the proposed framework and confirm the contributions made by the quality-aware features extracted from dynamic views.

**Index Terms**—point cloud quality assessment, moving camera videos, no-reference, video quality assessment

## I. INTRODUCTION

**P**oint cloud is essentially a huge collection of tiny individual points plotted in 3D space and each point is represented with the geometry coordinates and may be attached with color or texture. With the rapid development of computer graphics, point cloud has gained a better ability to vividly describe virtual objects and has been widely employed in diverse applications such as virtual reality [1], 3D reconstruction [2], and metaverse [3]. Nevertheless, the visual quality of point clouds can be affected by a variety of distortions. For example, point clouds are usually generated by the 3D laser scanner [4], thus disturbances such as noise and slight shifts may be introduced to the constructed point clouds. Moreover, to

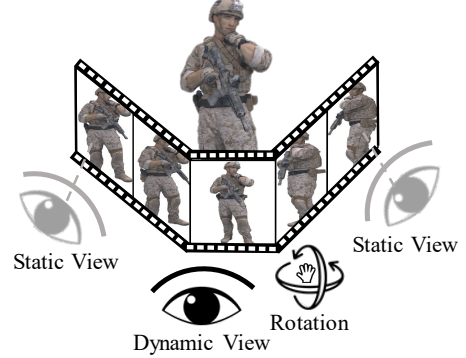


Fig. 1. Illustration of human habit of observing point cloud via static and dynamic views. The static views focus on the single rendered images while the dynamic views focus on the frames (usually generated by rotation).

reduce the storage consumption as well as transmission pressure, most point clouds are processed with lossy compression and downsampling, which inevitably damages the perceived quality of point clouds [5]–[8]. Therefore, it is necessary to carry out objective point cloud quality assessment (PCQA) metrics to automatically reflect the visual quality levels of point clouds.

In the last decade, large amounts of PCQA methods have been proposed [9]–[21], which can be generally categorized into full-reference (FR), reduced-reference (RR), and no-reference (NR) PCQA methods according to the involve extent of reference information. In many practical situations such as 3D reconstruction, the pristine reference point cloud is not available, thus NR-PCQA methods have wider application, which is also the focus of this paper. Moreover, NR-PCQA methods can be divided into model-based and projection-based methods as well. The model-based methods make evaluation directly from the point cloud model [9], [10], [13], [22]–[26] while the projection-based methods assess the quality from the rendered 2D projections [27]–[29]. The model-based PCQA methods are more difficult to develop since the point clouds for quality assessment are usually complex and made up of large amounts of points, thus making it hard to efficiently extract quality-aware features. However, the model-based methods avoid information loss during the rendering process and are invariant to viewpoints. The projection-based PCQA methods in previous works mainly assess the quality by evaluating the 2D views from the separate and static viewpoints [27], [29]. Such methods are based on the assumption that humans perceive the quality of point clouds through fixed static views. However, this hypothesis does not fully hold in the practical

Zicheng Zhang, Wei Sun, Xiongkuo Min, Yu Fan, and Guangtao Zhai are with the Institute of Image Communication and Network Engineering, Shanghai Jiao Tong University, 200240 Shanghai, China. E-mail: {zzc1998, sunguwei, minxiongkuo, fy-sky, zhaiguangtao}@sjtu.edu.cn.

The code will be available at [https://github.com/zzc-1998/VQA\\_PC](https://github.com/zzc-1998/VQA_PC).

situation. As illustrated in Fig. 1, humans tend to observe the point cloud through the combination of static views and dynamic rotation, in which the temporal features can have an impact on the subjective judgment as well. What’s more, the same type of distortions may have different visual quality difference between the static and dynamic views. Thus we come to the hypothesis that the perceived visual quality of the point clouds can be better evaluated by jointly making use of static and dynamic views.

To achieve this end, in this paper, we propose to treat point cloud as moving camera videos and infer the point cloud quality through the quality-aware static (spatial) and dynamic (temporal) information from the corresponding videos. More specifically, the spatial features of point cloud videos help describe the annoyance of distortions in static state. While the temporal features of point cloud videos assist to explore the influence of content changes among continuous viewpoints and tell whether the changes are abrupt and unpleasing under certain distortions. For example, as shown in Fig. 2, the undesired geometric deformation is obviously abrupt among frames and the color noise makes the content difference between the adjacent frames more incoherent, even resulting in flickering. Driven by such motivation, we first rotate the camera around the point cloud through four circular pathways to capture four video clips to cover sufficient quality-aware content. Each clip has 30 frames and we stitch the four clips into a video consisting of 120 frames. Second, following the strategies in common VQA methods [30], [31], we extract the spatial and temporal features from selected key frames and video clips by utilizing trainable 2D-CNN and pre-trained 3D-CNN models. Then the obtained spatial and temporal features are processed with linear projection to align the number of channels and then concatenated to form the final quality-aware features. In the last, the features are regressed into quality values using fully-connected (FC) layers. The experimental results show that the proposed method significantly outperforms the NR-PCQA and is even comparable compared with FR-PCQA methods. The major contributions of this paper are summarized as follows:

- We deal with the PCQA tasks with VQA methods by treating point cloud as moving camera videos, which push forward the development of projection-based PCQA methods by taking advantage of both static and dynamic views.
- We design a video capture framework for point cloud. The camera is rotated around the point cloud via four symmetric circular pathways to cover sufficient quality-aware content.
- The proposed method and baseline PCQA methods are validated on the SJTU-PCQA [27], the WPC [32], and the LSPCQA-I [33] databases. Extensive experimental results show that the proposed method significantly outperforms all compared NR methods and is even comparable with FR methods. Further ablation studies verify the effectiveness of the proposed structure and confirm the improvement made by dynamic views.

The rest of the paper is organized as follows. Section II briefly summarizes the development of PCQA and VQA

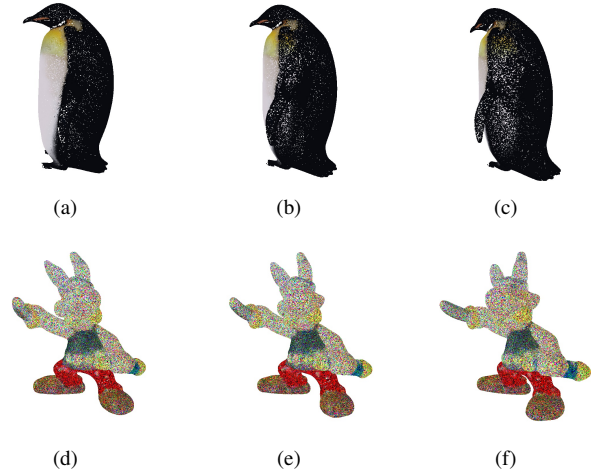


Fig. 2. Distortion reflection among dynamic views. (a), (b), and (c) are frames of the point cloud with downsampling distortion while (d), (e), and (f) are frames the point cloud with color noise.

methods. Section III describes the process of video capture, feature extraction, and feature regression. Section IV gives the performance results of the proposed methods and the comparing methods. In-depth discussions are given as well. Section V concludes this paper.

## II. RELATED WORK

In this section, we give a brief discussion about the development of point cloud quality assessment (PCQA) and video quality assessment (VQA).

### A. PCQA Development

The PCQA is still an emerging field in the current literature. The earliest PCQA methods simply focus on the point level, which include p2point [9], p2plane [10], and p2mesh [13]. The p2point calculates the distance between corresponding points to infer the distortion levels, the p2plane utilizes the projection of the distance vector along an average normal vector, and the p2mesh computes the distance from points to the reconstructed surface after mesh reconstruction to estimate the quality loss. However, these methods only take geometry information into consideration, thus obtaining unsatisfying performance in the latest colored PCQA databases [27], [29]. Then PointSSIM [22] predicts the quality difference between the reference and distorted point clouds by comparing the local topology and color distributions. GraphSIM [23] infers point cloud quality through graph similarity and color gradient. To further take advantage of various features, PCQM [24] employs a weighted linear combination of curvature along with color features for evaluation. Besides, some researchers try to evaluate the visual quality of point clouds through 2D projections [27], [28], which achieves competitive performance with the assistance of mature IQA methods.

All the PCQA methods mentioned above are FR methods, which require the involvement of reference point clouds, thus having a smaller range of applications. However, limited numbers of NR-PCQA methods have been proposed. ResCNN [34]

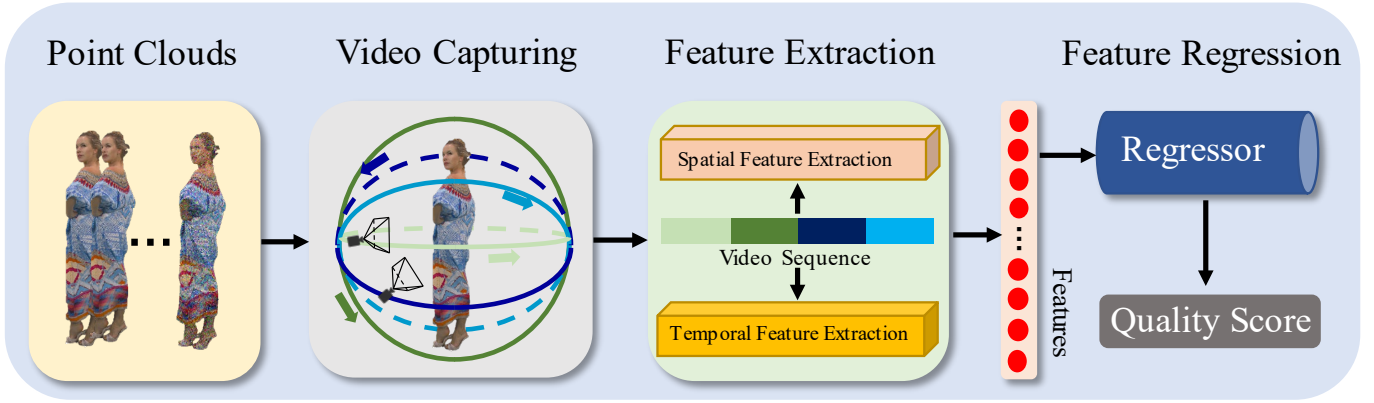


Fig. 3. The framework of the proposed method, which includes the video capture process, the feature extraction module, and the feature regression module.

designs an end-to-end sparse convolutional neural network to extract quality-aware features. PQA-net [29] classifies and evaluates the distortions by multi-view-based joint feature extraction. 3D-NSS [26] employs both geometry and color attributes and utilizes some well-behaving distribution models for analysis.

### B. VQA Development

FR-VQA methods usually compute the quality difference between the reference and distorted frames with IQA methods (commonly using PSNR, SSIM [35]) to represent the video quality. With the development of machine learning, Video Multi-Method Assessment Fusion (VMAF) [36] proposed by Netflix extracts various IQA features along with temporal features and uses Support Vector Regressor (SVR) for quality regression.

Similar to the strategy employed in FR-VQA methods, a simple NR-VQA method is to compute each frame's quality level using NR IQA methods (such as NIQE [37]) and obtain the video quality via average pooling. To further incorporate spatial as well as temporal features, many handcrafted-based methods have been proposed to extract spatio-temporal features from the video [38]–[41]. Considering the huge success of deep learning, deep neural networks (DNN) have been employed for VQA tasks as well. VSFA [42] extracts quality-aware features with a pre-trained DNN model and models the temporal effect with gated recurrent units (GRUs). Rapique [43] combines and leverages the advantages of both quality-aware scene statistics features and semantics-aware deep features for video quality prediction. StairVQA [44] further utilizes both low-level and high-level information as video quality representation. To better understand video distortions caused by the motion effect, some studies [30], [31] attempt to extract temporal features with 3D-CNN models pre-trained on the video action recognition databases to enhance video quality understanding and have achieved strong performance.

## III. PROPOSED METHOD

The framework of the proposed method is clearly exhibited in Fig. 3, which includes the video capture module, the feature extraction module, and the feature regression module.

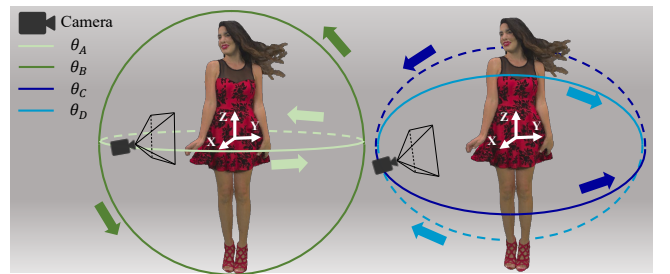


Fig. 4. Illustration of videos capturing process via moving camera. The point cloud sample is *redandblack* from the SJTU-PCQA database [27].  $\theta_A$ ,  $\theta_B$ ,  $\theta_C$ , and  $\theta_D$  represent the four moving paths respectively.

### A. video capture

1) *Pathways*: Given a point cloud  $\mathbf{P} = \{\delta_m, \gamma_m\}_{m=1}^N$ , where  $\delta_m \in \mathbb{R}^{1 \times 3}$  indicates the geometry coordinates,  $\gamma_m \in \mathbb{R}^{1 \times 3}$  represents the attached RGB color information, and  $N$  stands for the number of points. The corresponding video sequence  $\mathbf{V}$  is generated with the assistance of the Python package `open3d` [45]:

$$\mathbf{V} = \Psi(\mathbf{P}), \quad (1)$$

where the  $\Psi(\cdot)$  indicates the video capture operation. Specifically, the camera is first placed at the default position with a fixed viewing distance  $R$ . Then we define the geometry mean center of the point cloud  $\mathbf{P}$  as:

$$O_\delta = \frac{1}{N} \sum_{m=1}^N \delta_m, \quad (2)$$

where the  $O_\delta$  represents the  $(X, Y, Z)$  coordinates of the point cloud's mean center,  $N$  denotes the number of the points, and  $\delta_m$  stands for the  $(X, Y, Z)$  coordinates of the  $m$ -th point in the point cloud. Next, we establish a space Cartesian coordinate system with  $O_\delta$  as the center and the position coordinates of the moving camera are defined as  $(X_\alpha, Y_\alpha, Z_\alpha)$ . To cover as much quality-aware content as possible, we especially design 4 symmetric circular rotation pathways to model the temporal features of the point cloud, which can be represented as:

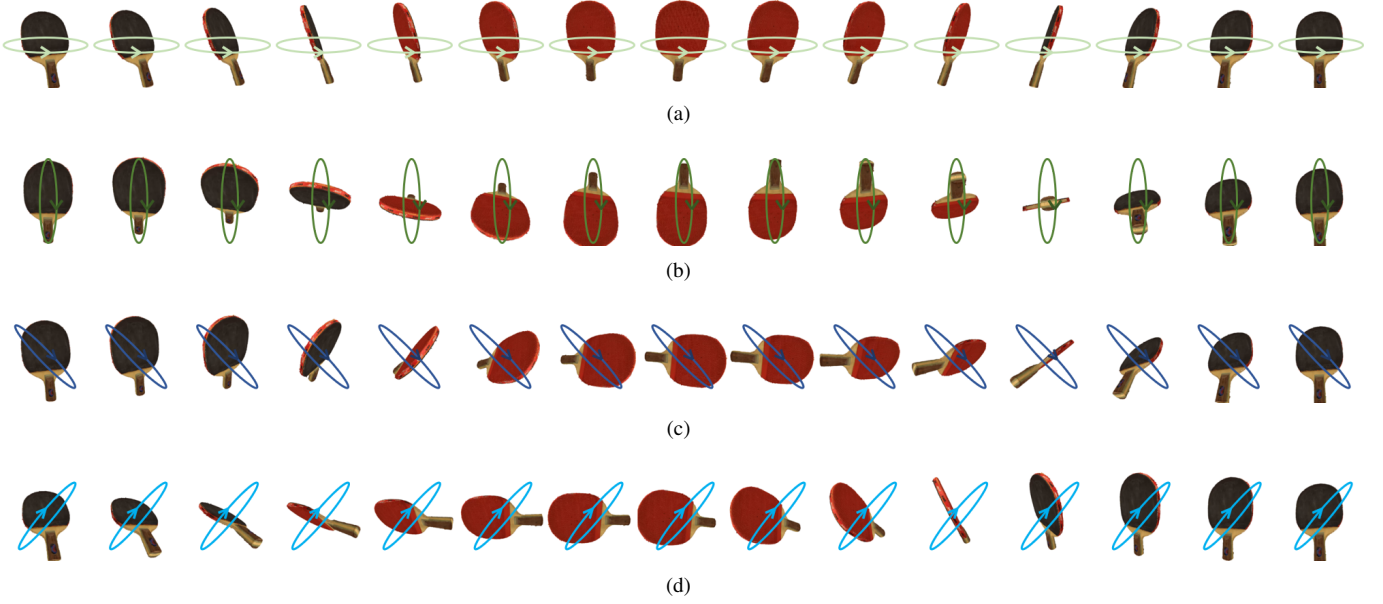


Fig. 5. Example of the captured video from the point cloud *ping\_pong\_bat* from the WPC database [32], where (a), (b), and (c) represent the samples frames captured of  $\theta_A$ ,  $\theta_B$ ,  $\theta_C$ , and  $\theta_D$  respectively.

$$\theta_A : \begin{cases} X_\alpha^2 + Y_\alpha^2 = R^2, \\ Z_\alpha = 0, \end{cases}$$

$$\theta_B : \begin{cases} Y_\alpha^2 + Z_\alpha^2 = R^2, \\ X_\alpha = 0, \end{cases}$$

$$\theta_C : \begin{cases} X_\alpha^2 + Y_\alpha^2 + Z_\alpha^2 = R^2, \\ X_\alpha + Z_\alpha = 0, \end{cases}$$

$$\theta_D : \begin{cases} X_\alpha^2 + Y_\alpha^2 + Z_\alpha^2 = R^2, \\ X_\alpha - Z_\alpha = 0, \end{cases} \quad (6)$$

where  $\theta_A$ ,  $\theta_B$ ,  $\theta_C$ , and  $\theta_D$  represent the four corresponding pathways,  $R$  indicates the radius of the circle. The illustration of the video capture process is clearly shown in Fig. 4.

2) *Camera Rotation*: To maintain the consistency of the videos, the camera rotation step is set as  $12^\circ$  between consecutive frames through trial. To be more specific, the camera rotates  $12^\circ$  around the center of the circular pathway to capture the next frame after capturing the current frame. Then a clip of  $360/12 = 30$  frames is captured to cover each circular pathway, and a video consisting of four clips and  $4 \times 30 = 120$  frames is obtained for the point cloud. In addition, the camera returns to the same starting position after sampling frames for each pathway, therefore, the captured video is continuous among the clips. An example of the captured video is presented in Fig. 5, from which we can distinctly observe the rotation changes reflected through the four pathways.

## B. Feature Extraction

Similar to most VQA methods, we try to extract the quality-aware information based on the spatial and temporal aspects. Therefore, inspired by previous VQA models [30], [31], we

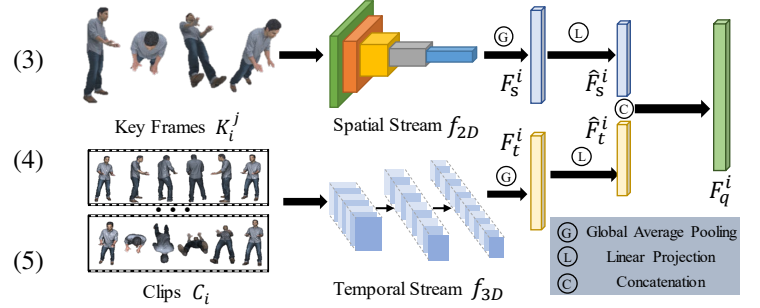


Fig. 6. The detailed structure of the feature extraction.

utilize a 2D and 3D combined approach as the structure of the feature extraction, which is illustrated in Fig. 6. Following the video capture process described above, we can obtain a video sequence  $\mathbf{V}$  with four clips  $\{C_i\}_{i=1}^4$  according to the four pathways and each clip is composed of 30 frames. Then a key frame  $K_i^j$  ( $j$  is the frame index within the clip,  $0 \leq j < 30$ ) chosen in each single clip  $C_i$  is selected for spatial feature extraction while each whole single clip  $C_i$  is employed for the temporal feature extraction respectively.

1) *Spatial Feature Extraction*: Given a key frame  $K_i^j$ , we simply use a trainable 2D-CNN model to extract the spatial feature maps:

$$\begin{aligned} F_s^i &= f_{2D}(K_i^j), \\ \hat{F}_s^i &= \text{GAP}(F_s^i), \end{aligned} \quad (7)$$

where  $f_{2D}(\cdot)$  denotes the 2D-CNN model,  $F_s^i \in \mathbb{R}^{C \times H \times W}$  represents the spatial feature maps for  $K_i^j$ ,  $\text{GAP}(\cdot)$  indicates the global average pooling function, and  $\hat{F}_s^i \in \mathbb{R}^{C_s \times 1}$  stands for the averaged spatial feature representation.

2) *Temporal Feature Extraction*: Unlike the spatial features focusing on single frames, temporal features pay more attention to the relations between intermediate frames, which are

therefore more capable of reflecting the perceptual distortions in a dynamic manner. To extract the temporal features, we employ the pre-trained 3D-CNN model as the temporal feature extractor, which has been a common approach in many VQA studies [30], [31]. Moreover, the feature representation acquired by the pre-trained 3D-CNN model is believed to have a strong ability to capture the effect of content changes and model the motion information that is highly correlated with the human vision system (HVS) [30]. In addition, the temporal features are not sensitive to the resolution and we downsample the clips to a low resolution before temporal feature extraction. Given the clip  $C_i$  and the pre-trained 3D-CNN model, the temporal features can be derived as:

$$\begin{aligned} F_t^i &= f_{3D}(C_i), \\ \hat{F}_t^i &= \text{GAP}(F_t^i), \end{aligned} \quad (8)$$

where  $f_{3D}(\cdot)$  stands for the pre-trained 3D-CNN model,  $\hat{F}_t^i \in \mathbb{R}^{C_t \times 1}$  is the temporal quality-aware feature representation after global averaging pooling.

3) *Feature Fusion*: Since the number of output channels of spatial features and temporal features usually differ from each other, the linear projection is utilized to align the number of channels. Then the spatial and temporal features are concatenated to form the final quality-aware features:

$$F_q^i = W_s \hat{F}_s^i \oplus W_p \hat{F}_t^i, \quad (9)$$

where  $W_s$  and  $W_p$  are learnable linear mappings,  $W_s \hat{F}_s^i$  and  $W_p \hat{F}_t^i \in \mathbb{R}^{C' \times 1}$  ( $C'$  is the number of aligned channels),  $\oplus$  indicates the concatenation operation,  $F_q^i \in \mathbb{R}^{2C' \times 1}$  represents the combined quality-aware feature for clip  $C_i$ .

To sum up, we select a key frame  $K_i^j$  from the clip  $C_i$  for the spatial feature extraction and we use the whole clip  $C_i$  for the temporal feature extraction. Finally, the quality-aware features  $F_q^i$  for clip  $C_i$  are obtained via the linear projection and concatenation.

### C. Feature Regression

With the generated quality-aware features, we employ a two stage fully-connected (FC) layers consisting of 128 and 1 neuron respectively for feature regression, which can be derived as:

$$Q_i = \text{FC}(F_q^i), \quad (10)$$

where  $\text{FC}(\cdot)$  denotes the FC layers and  $Q_i$  stands for the quality score for the  $i$ -th clip  $C_i$ . Considering that each video includes four clips, we generate the overall quality score through average pooling:

$$Q = \frac{1}{4} \sum_{i=1}^4 Q_i, \quad (11)$$

where  $Q$  represents the predicted quality level for the video.

### D. Loss Function

To directly investigate the effectiveness of the VQA application for the point cloud, we directly use the Mean Squared Error (MSE) as the loss function:

$$\text{Loss} = \frac{1}{n} \sum_{l=1}^n (L_\eta - Q_\eta)^2 \quad (12)$$

where  $n$  indicates the number of videos in a mini-batch,  $L_\eta$  and  $Q_\eta$  are the subjective quality labels and predicted quality levels respectively.

## IV. EXPERIMENT

In this section, we give the details of the experimental setup. We select several state-of-the-art PCQA and VQA methods for comparison. Further ablation studies are carried out to verify the effectiveness of the proposed method.

### A. Experiment Setup

1) *Benchmark Databases*: We mainly validate the effectiveness of the proposed method on the subjective point cloud assessment database (SJTU-PCQA) [27], the Waterloo point cloud assessment database (WPC) [32], and the large-scale point cloud quality assessment database part I (LSPCQA-I) [33]. The SJTU-PCQA database provides 10 groups of distorted point clouds generated from 10 reference point clouds and 9 groups of point clouds are publicly available. Each group contains 42 distorted point clouds obtained from seven kinds of synthetic distortions with six strengths, which generates  $9 \times 42 = 378$  distorted point clouds in total. The WPC database includes 740 distorted point clouds generated from 20 reference point clouds by manually introducing downsampling, Gaussian noise, and three types of compression distortions. The LSPCQA-I database is made up of 930 distorted point clouds generated with 5 distortion levels of 31 types of distortions. More complex distortions such as contrast distortion, Gamma noise, mean shift, local missing, etc. are introduced to this database, which makes the LSPCQA-I database more challenging.

2) *Comparing Models*: The comparing PCQA methods can be divided into two categories:

- *Model-based methods*: The methods assess the visual quality of distorted point clouds directly from the 3D digital representation. The FR model-based methods include GraphSIM [46], PointSSIM [17], and PCQM [20]. The RR model-based methods include PCMRR [47]. The NR model-based methods include 3D-NSS [26].
- *Projection-based methods*: The projection-based methods evaluate the visual quality of point clouds via the rendered 2D projections. The FR projection-based methods consist of PSNR and SSIM [35]. The NR projection-based methods include BRISQUE [48], NIQE [37], PQA-net [29], VIIDEO [38], V-BLIINDS [39], TLVQM [40], VIDEVAL [41], VSFA [42], RAPIQUE [43], and StairVQA [44]. It's worth mentioning that PSNR, SSIM, NIQE, and BRISQUE are IQA methods and we validate these methods by averaging the frames' quality scores.

TABLE I  
PERFORMANCE RESULTS ON THE SJTU-PCQA, WPC, AND LSPCQA-I DATABASES. THE BEST PERFORMANCE RESULTS ARE MARKED IN RED AND THE SECOND PERFORMANCE RESULTS ARE MARKED IN BLUE.

Ref	Type	Index	Methods	SJTU-PCQA				WPC				LSPCQA-I			
				SRCC↑	PLCC↑	KRCC↑	RMSE↓	SRCC↑	PLCC↑	KRCC↑	RMSE↓	SRCC↑	PLCC↑	KRCC↑	RMSE↓
FR	Model-based	A	PCQM	<b>0.8644</b>	<b>0.8853</b>	<b>0.7086</b>	<b>1.0862</b>	<b>0.7434</b>	<b>0.7499</b>	<b>0.5601</b>	15.1639	0.3911	0.4044	0.3119	0.7527
		B	GraphSIM	<b>0.8783</b>	0.8449	<b>0.6947</b>	<b>1.0321</b>	0.5831	0.6163	0.4194	17.1939	0.3112	0.3774	0.2166	0.7426
		C	PointSSIM	0.6867	0.7136	0.4964	1.7001	0.4542	0.4667	0.3278	20.2733	0.3155	0.5346	0.2443	0.7564
	Projection-based	D	PSNR	0.2952	0.3222	0.2048	2.2972	0.1261	0.1801	0.0897	22.5482	0.5580	0.5909	0.3989	0.6640
		E	SSIM	0.3850	0.4131	0.2630	2.2099	0.2393	0.2881	0.1738	21.9508	0.5564	0.5580	0.3815	0.6129
RR	Model-based	F	PCMRR	0.4816	0.6101	0.3362	1.9342	0.3097	0.3433	0.2082	21.5302	0.1673	0.1650	0.1153	0.8086
NR	Model-based	G	3D-NSS	0.7144	0.7382	0.5174	1.7686	0.6479	0.6514	0.4417	16.5716	0.4509	0.4751	0.3180	0.7317
	Projection-based	H	BRISQUE	0.3975	0.4214	0.2966	2.0937	0.2614	0.3155	0.2088	21.1736	0.2910	0.2951	0.1227	0.8038
		I	NIQE	0.1379	0.2420	0.1009	2.2622	0.1136	0.2225	0.0953	23.1415	0.1127	0.2577	0.0797	0.7982
		J	PQA-net	-	-	-	-	0.7034	0.7113	0.4956	15.0210	0.5711	0.5616	0.4127	0.6181
		K	VIIDEO	0.0509	0.2960	0.0433	2.3180	0.0775	0.0823	0.0538	22.9231	0.0733	0.2066	0.0511	0.8030
		L	V-BLIINDS	0.6804	0.7822	0.4863	1.5091	0.4618	0.4903	0.3096	19.7348	0.2008	0.2439	0.1372	0.8071
		M	TLVQM	0.5270	0.6081	0.3442	1.9125	0.0366	0.0191	0.2081	22.1481	0.3381	0.3997	0.2324	0.7628
		N	VIDEAL	0.6027	0.7465	0.4259	1.5079	0.3744	0.2653	0.3630	21.0992	0.3676	0.4249	0.2575	0.7533
		O	VSFA	0.7233	0.8230	0.5477	1.4096	0.6355	0.6331	0.4649	17.2344	0.5557	0.5659	0.4124	0.6542
		P	RAPIQUE	0.4441	0.4054	0.3417	2.2144	0.2793	0.3577	0.2062	21.1455	0.3787	0.4130	0.2624	0.7579
		Q	StairVQA	0.7812	0.7744	0.5635	1.4564	0.7314	0.7239	0.5584	<b>14.1723</b>	<b>0.6013</b>	<b>0.6243</b>	<b>0.4508</b>	<b>0.6109</b>
	R	Proposed	0.8509	<b>0.8635</b>	0.6585	1.1334	<b>0.7968</b>	<b>0.7976</b>	<b>0.6115</b>	<b>13.6219</b>	<b>0.6950</b>	<b>0.7151</b>	<b>0.5151</b>	<b>0.5855</b>	

The VIIDEO, V-BLIINDS, TLVQM, VIDEVAL, VSFA, RAPIQUE, and StairVQA are VQA methods, among which VIIDEO, V-BLIINDS, TLVQA, and VIDEAL are handcrafted-based methods while VSFA, RAPIQUE, and StairVQA are DNN-based methods.

We employ the k-fold cross validation strategy for experiment as suggested in [49], [50]. For the SJTU-PCQA database, we select 8 groups of point clouds for training and leave 1 group for testing. Such split process is repeated 9 times so that each group of point cloud is exactly tested only once. For the WPC database, we divide the 20 groups of point clouds into 5 folds and each fold consists of 4 groups of point clouds. Then the similar testing process is utilized. For the LSPCQA-I database, the same 5 fold cross validation is employed as well. The average performance of the k folds is recorded as the final experimental results. It's worth noting that there is no content overlap between the training and testing sets. We strictly retrain the compared NR-PCQA methods utilizing the same training and testing sets splits. What's more, for the FR-PCQA and RR-PCQA methods that require no training, we simply validate these methods on the same testing sets and report the average performance to make the comparison even.

3) *Evaluation Criteria*: We employ four common consistency evaluation criteria to judge the correlation between the predicted scores and MOSs, which consist of Spearman Rank Correlation Coefficient (SRCC), Kendall's Rank Correlation Coefficient (KRCC), Pearson Linear Correlation Coefficient (PLCC), and Root Mean Squared Error (RMSE). An excellent model should get SRCC, KRCC, and PLCC values as close as possible to 1, and get the RMSE value as close as possible

to 0.

Additionally, to deal with the scale differences between the predicted quality scores and the quality labels among different PCQA methods, a five-parameter logistic function is employed to map the predicted scores before computing the criteria values:

$$\hat{y} = \beta_1 \left( 0.5 - \frac{1}{1 + e^{\beta_2(y - \beta_3)}} \right) + \beta_4 y + \beta_5, \quad (13)$$

where  $\{\beta_i \mid i = 1, 2, \dots, 5\}$  are parameters to be fitted,  $y$  and  $\hat{y}$  are the predicted scores and mapped scores respectively.

4) *Implementation Details*: Specifically, the ResNet50 [51] is used as the spatial feature extractor. The key frame index is set as 5, which indicates that the 5-th frame of each clip is used for spatial feature extraction. Since the spatial features are sensitive to the resolution, we maintain the original resolution ( $1920 \times 1080 \times 3$ ) of the key frames. Patches with the resolution of  $224 \times 224 \times 3$  are randomly cropped from the key frames for training while patches with the same resolution are cropped in the center for testing. The SlowFast R50 [52] is utilized as the temporal feature extractor and only the fast pathways are used. The clips are resized to  $224 \times 224$  for both training and testing. Additionally, the ResNet50 is initialized with the pre-trained model on the ImageNet database [53] and is fine-tuned during the training stage. The SlowFast R50 is frozen with the weights of the pre-trained model on the Kinetics 400 database [54]. The adam optimizer [55] is employed. The default batch size is set as 32 and the default training epochs are set as 50. The initial learning rate is set as  $5e-5$ , which decays with a ratio of 0.9 for every 10 epochs.

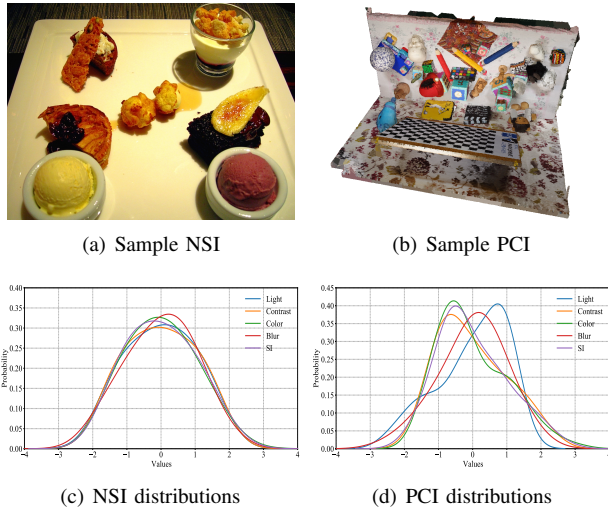


Fig. 7. The normalized probability distributions of 5 quality-related attributes for NSIs and PCIs. The quality-related attributes include light, contrast, colorfulness, blur, and spatial information (SI), the details description of which can be referred to in [56]. The distributions are obtained from 10,073 NSIs in the KonIQ-10k IQA database [57] and  $(374+740) \times 120 = 134,160$  PCIs rendered from the SJTU-PCQA database [27] and the WPC database [32] respectively. The ‘color’ indicates the colorfulness of the images and the ‘SI’ stands for the texture diversity of the images.

### B. Performance Discussion

The final experimental results on the SJTU-PCQA, WPC, and LSPCQA-I databases are clearly shown in Table I, from which we can make several observations. a) The proposed method achieves the third place on the SJTU-PCQA database (about 0.03 behind the first place), the first place on the WPC database (surpass the second place by about 0.05), and the first place on the LSPCQA-I database (surpass the second place by about 0.09) among all the comparison methods in terms of SRCC, which verifies the effectiveness of the proposed method for predicting the visual quality levels of point clouds. b) The model-based FR methods achieve relatively better performance, which is because these methods take advantage of reference information and extract features directly from the point cloud. c) The handcrafted-based NR-VQA methods seem to be less competent for giving the quality values of point clouds. We attempt to give the reasons for such phenomenon. Most handcrafted-based NR-VQA methods are specially developed to tackle the quality assessment for natural scene content. For example, BRISQUE and NIQE operate by measuring the deviations from statistical regularities observed in natural images, however, the statistical regularities do not hold for the point cloud rendering images (PCIs). As can be seen from Fig. 7, PCIs usually contain more geometric shapes, simpler texture, and less colors, which differ greatly from the NSIs in statistics. Therefore, such handcrafted-based NR methods are not suitable for extracting quality-aware information from point cloud projections, which results in lower performance. d) The DNN-based NR-VQA methods except RAPIQUE (RAPIQUE utilizes pre-trained DNN models, thus resulting in poor performance) achieve more impressive performance. Specifically, VSFA, StairVQA, and the proposed method are the top 3 among the NR methods on the SJTU-

TABLE II  
PERFORMANCE RESULTS OF THE ABLATION STUDY ON THE SJTU-PCQA AND WPC DATABASES. THE BACKBONES MARKED WITH \* ARE THE PROPOSED SELECTION. × INDICATES THAT NO BACKBONE IS USED. BEST IN BOLD.

Backbone		SJTU-PCQA		WPC	
Spatial	Temporal	SRCC↑	PLCC↑	SRCC↑	PLCC↑
ResNet50	×	0.8157	0.8413	0.7693	0.7715
×	SlowFast	0.3443	0.5985	0.1815	0.2509
ResNet50	X3D	0.8441	<b>0.8958</b>	0.7785	0.7715
ResNet34	SlowFast	0.8294	0.8944	0.7764	0.7743
ResNet50*	SlowFast*	<b>0.8509</b>	0.8635	<b>0.7968</b>	<b>0.7976</b>
ResNet101	SlowFast	0.8303	0.8301	0.7791	0.7874
VGG16	SlowFast	0.8205	0.8927	0.7558	0.7682
MobileNetV2	SlowFast	0.8273	0.8550	0.7544	0.7650

PCQA and LSPCQA-I databases in terms of SRCC. This is because these methods employ powerful DNN models to learn the quality representation from both the static and dynamic views, which validates our motivation that the perceived visual quality of point clouds can be better modeled via moving camera videos. e) All methods experience a clear performance drop on the WPC and LSPCQA-I databases compared with the SJTU-PCQA database. It can be explained that the WPC and LSPCQA-I databases are more diverse in contents and distortion types. What’s more, the distortion gaps for the SJTU-PCQA database are relatively coarse-grained, thus making it easier for the PCQA models to distinguish quality differences. However, the proposed method yields the best performance on the more challenging WPC and LSPCQA-I databases, which further demonstrates the effectiveness of the proposed method.

### C. Ablation Study

Since the proposed method incorporates both temporal and spatial information for quality prediction, we try to quantify the contributions of temporal and spatial components. In addition, we replace the 2D-CNN and 3D-CNN backbones with other mainstream models for validation. Specifically, we replace the ResNet50 backbone with ResNet34, ResNet101 [51], VGG16 [58], and MobileNetV2 [59] as spatial feature extractor. We replace the pre-trained SlowFast model [52] with the pre-trained X3D [60] as the temporal feature extractor. The default experimental setup is maintained and the experimental results are shown in Table II. First, the separate ResNet50 and SlowFast models are inferior to the proposed model, which implies that both spatial and temporal information make contributions. With closer inspections, the spatial information makes more contributions to the final results. Second, by comparing the performance of different backbones, the proposed selection is optimal for the PCQA tasks on the validated databases. Finally, although models employing other mainstream backbones achieve lower performance than the proposed method, they are still competitive among the previously developed PCQA methods, which further verifies the effectiveness of the proposed structure.

TABLE III

PERFORMANCE RESULTS OF DIFFERENT KEY FRAME SELECTION ON THE SJTU-PCQA AND WPC DATABASES. THE FRAME INDEX MARKED WITH \* ARE THE PROPOSED SELECTION. BEST IN BOLD.

Database	SJTU-PCQA		WPC	
	Frame Index	SRCC $\uparrow$	PLCC $\uparrow$	SRCC $\uparrow$
5-th*	<b>0.8509</b>	<b>0.8635</b>	<b>0.7968</b>	0.7976
10-th	0.8458	0.8490	0.7922	0.7854
15-th	0.8445	0.8516	0.7962	0.7807
20-th	0.8493	0.8629	0.7853	0.7895
25-th	0.8501	0.8493	0.7911	<b>0.7988</b>
30-th	0.8113	0.8216	0.7791	0.7874

TABLE IV

PERFORMANCE RESULTS OF PATHWAY COMPARISON ON THE SJTU-PCQA AND WPC DATABASES. THE MARK  $\checkmark$  IN THE PATHWAYS COLUMN INDICATES THAT THE CORRESPONDING PATHWAY IS USED. BEST IN BOLD.

Model	Pathway				SJTU-PCQA		WPC	
	$\theta_A$	$\theta_B$	$\theta_C$	$\theta_D$	SRCC $\uparrow$	PLCC $\uparrow$	SRCC $\uparrow$	PLCC $\uparrow$
P1	$\checkmark$	$\times$	$\times$	$\times$	0.7812	0.8409	0.7120	0.7190
P2	$\checkmark$	$\checkmark$	$\times$	$\times$	0.8203	0.8411	0.7477	0.7327
P3	$\checkmark$	$\checkmark$	$\checkmark$	$\times$	0.8295	0.8464	0.7726	0.7769
P4	$\checkmark$	$\checkmark$	$\times$	$\checkmark$	0.8424	0.8621	0.7849	0.7734
P5	$\checkmark$	$\times$	$\checkmark$	$\checkmark$	0.8471	<b>0.8694</b>	0.7584	0.7693
P6	$\times$	$\checkmark$	$\checkmark$	$\checkmark$	0.8373	0.8641	0.7634	0.7688
P7	$\checkmark$	$\checkmark$	$\checkmark$	$\checkmark$	<b>0.8509</b>	0.8635	<b>0.7968</b>	<b>0.7976</b>

#### D. Key Frame Selection

In the feature extraction, a key frame is selected among each clip as the spatial input. In this section, we try to find out the influence caused by different key frame selection. The default experimental setup is maintained and we manually choose the 5-th, 10-th, 15-th, 20-th, 25-th, and 30-th frame of each clip as the key frame for validation. The experimental results are shown in Table III, from which we can observe that the selection of key frames has slight influence on the final results except for choosing the 30-th frame. When choosing the 30-th frame of each clip as the key frame, the performance is obviously lower than other selection. It is because the camera returns to the same starting point after each clip and the 30-th frame is captured from close viewpoints, thus covering less content than other selection.

#### E. Pathway Comparison

The proposed method employs four pathways to capture videos. Although the pathways are quite different, the capture clips may still share similar visual contents. It is necessary to investigate whether there is redundancy among the pathways and quantify the contributions of each pathway. Therefore, in this section, we use 3, 2, and 1 pathways for the experiment and list the performance results in Table IV. First, by comparing the performance of model P1  $\sim$  P3, it can be viewed that the experimental performance is consistently improved with the increasing number of pathways, which indicates that capturing more video clips is beneficial for enhancing the qual-

TABLE V

THE DETAILED TIME COST OF COMPARING PCQA METHODS.

Method	PCQM	GraphSIM	PointSSIM	PCMRR	3D-NSS	Proposed
Time/s	17.63	304.64	10.63	62.53	5.68	13.15

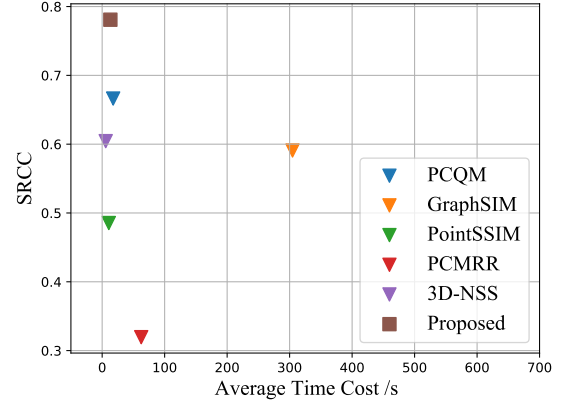


Fig. 8. The results of computational efficiency comparison. The SRCC indicates the average SRCC values of corresponding PCQA methods on the SJTU-PCQA, WPC, and LSPCQA-I databases. The average time cost represents the average running time of the PCQA methods to evaluate a single point cloud.

ity understanding of the model. Second, the P3  $\sim$  P6 models are all inferior to the P7 model, which implies that all four pathways make contributions to the final results. Moreover, the P6 model obtains the lowest performance among the P3  $\sim$  P6 models, which suggests that pathway  $\theta_A$  devotes more among the four pathways.

#### F. Computational Efficiency

Since the proposed method needs to first capture the videos and then predict the visual quality of point clouds from the video, we are also interested in the computational efficiency of the proposed method. Considering that the projection-based methods share the time consumption of generating videos, we mainly select the model-based methods for comparison, which include PCQM, GraphSIM, PointSSIM, PCMRR, and 3D-NSS. All the algorithms are implemented on a laptop with AMD Ryzen 7 5800H @ 3.20 GHz CPU, 16G RAM, and NVIDIA Geforce RTX 3050Ti GPU on the Windows platform. We report the average running time per point cloud on the SJTU-PCQA, WPC, and LSPCQA-I databases for each PCQA method. It's worth mentioning that the running time for the proposed method includes the video capture time consumption and inference time consumption. The computational efficiency comparison results are illustrated in Fig. 8 and the detailed time cost is listed in Table V. Although PointSSIM and 3D-NSS take less time than the proposed method, their performance is considerably lower than the proposed method. The proposed method achieves first place on average SRCC values while maintaining competitive computational efficiency, which implies the proposed method is capable of handling practical applications.

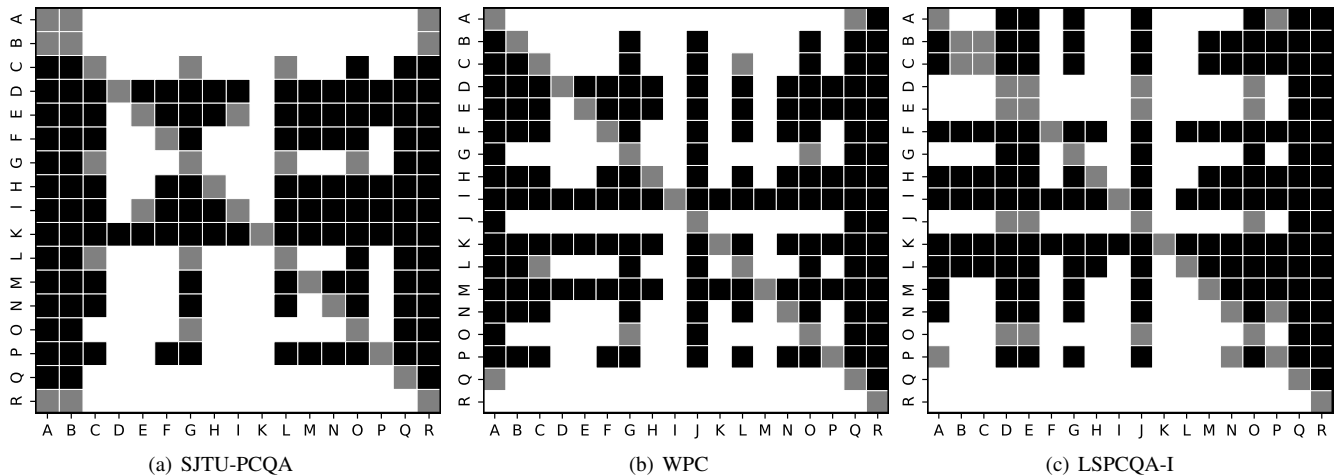


Fig. 9. Statistical test results of the proposed method and compared metrics on the SJTU-PCQA, WPC, and LSPCQA-I databases. A black/white block means the row method is statistically worse/better than the column one. A gray block means the row method and the column method are statistically indistinguishable. The metrics are denoted by the same index as in Table I.

### G. Statistical Test

To further analyze the performance of the proposed method, we conduct the statistical test in this section. We follow the same experimental setup as in [61] and compare the difference between the predicted quality scores with the subjective ratings. All possible pairs of models are tested and the results are listed in Fig. 9. The method index is of the same order as in Fig. 1. It can be observed that the proposed method is significantly superior to most comparing methods. More specifically, the proposed method significantly outperforms 14, 17, and 17 compared methods on the SJTU-PCQA, WPC, and LSPCQA-I databases respectively. Additionally, the FR methods are insignificantly distinguishable from the proposed method on the SJTU-PCQA database while the proposed method achieves significantly better performance even than FR methods on the WPC and LSPCQA-I databases.

### V. CONCLUSION

This paper proposes a no-reference quality assessment method for point cloud by treating point cloud as moving camera videos. We hold the assumption that people tend to perceive the point cloud through both static and dynamic views. However, previous projection-based PCQA methods only evaluate the rendered 2D projections via fixed viewpoints. Therefore, the proposed method first generates the videos by rotating the camera along four designed pathways around the point clouds. Then the proposed method extracts spatial and temporal information from the key frames and video clips by employing trainable ResNet50 and pre-trained SlowFast R50 model. In this way, the proposed method is able to incorporate the quality-aware information from both static and dynamic views and gains an advantage over the previous projection-based PCQA methods. The experimental results show that the proposed method achieves significantly better performance than all NR-PCQA methods and the performance is even indistinguishable from FR-PCQA methods, which shows the effectiveness of the proposed method. Furthermore, the ablation study verifies the rationality of the proposed structure, and the detailed analysis is given as well.

### REFERENCES

- [1] J. Xiong, E.-L. Hsiang, Z. He, T. Zhan, and S.-T. Wu, "Augmented reality and virtual reality displays: emerging technologies and future perspectives," *Light: Science & Applications*, vol. 10, no. 1, pp. 1–30, 2021.
- [2] Z. Kang, J. Yang, Z. Yang, and S. Cheng, "A review of techniques for 3d reconstruction of indoor environments," *ISPRS International Journal of Geo-Information*, vol. 9, no. 5, p. 330, 2020.
- [3] H. Ning, H. Wang, Y. Lin, W. Wang, S. Dhelim, F. Farha, J. Ding, and M. Daneshmand, "A survey on metaverse: the state-of-the-art, technologies, applications, and challenges," *arXiv preprint arXiv:2111.09673*, 2021.
- [4] J.-Y. Chen, C.-H. Lin, P.-C. Hsu, and C.-H. Chen, "Point cloud encoding for 3d building model retrieval," *IEEE transactions on multimedia*, vol. 16, no. 2, pp. 337–345, 2013.
- [5] J.-Y. Sim and S.-U. Lee, "Compression of 3-d point visual data using vector quantization and rate-distortion optimization," *IEEE Transactions on Multimedia*, vol. 10, no. 3, pp. 305–315, 2008.
- [6] S.-B. Park and S.-U. Lee, "Multiscale representation and compression of 3-d point data," *IEEE Transactions on Multimedia*, vol. 11, no. 1, pp. 177–183, 2008.
- [7] A. Javaheri, C. Brites, F. Pereira, and J. Ascenso, "Point cloud rendering after coding: Impacts on subjective and objective quality," *IEEE Transactions on Multimedia*, vol. 23, pp. 4049–4064, 2020.
- [8] P. de Oliveira Rente, C. Brites, J. Ascenso, and F. Pereira, "Graph-based static 3d point clouds geometry coding," *IEEE Transactions on Multimedia*, vol. 21, no. 2, pp. 284–299, 2018.
- [9] P. Cignoni, C. Rocchini, and R. Scopigno, "Metro: Measuring error on simplified surfaces," *Computer Graphics Forum*, vol. 17, no. 2, pp. 167–174, 1998.
- [10] R. Mekuria and P. Cesar, "Mp3dgp-pcc, open source software framework for implementation and evaluation of point cloud compression." Association for Computing Machinery, 2016, p. 1222–1226.
- [11] G. Lavoué, "A multiscale metric for 3d mesh visual quality assessment," *Computer Graphics Forum*, vol. 30, no. 5, pp. 1427–1437, 2011.
- [12] K. Wang, F. Torkhani, and A. Montanvert, "A fast roughness-based approach to the assessment of 3d mesh visual quality," *Computers and Graphics*, vol. 36, no. 7, pp. 808–818, 2012.
- [13] D. Tian, H. Ochimizu, C. Feng, R. Cohen, and A. Vetro, "Geometric distortion metrics for point cloud compression," in *IEEE International Conference on Image Processing*, 2017, pp. 3460–3464.
- [14] E. Alexiou and T. Ebrahimi, "Point cloud quality assessment metric based on angular similarity," in *IEEE International Conference on Multimedia and Expo*, 2018, pp. 1–6.
- [15] A. Javaheri, C. Brites, F. Pereira, and J. Ascenso, "A generalized hausdorff distance based quality metric for point cloud geometry," in *International Conference on Quality of Multimedia Experience*, 2020, pp. 1–6.
- [16] L. Váša and J. Rus, "Dihedral angle mesh error: a fast perception correlated distortion measure for fixed connectivity triangle meshes," *Computer Graphics Forum*, vol. 31, no. 5, pp. 1715–1724, 2012.

- [17] E. Alexiou and T. Ebrahimi, "Towards a point cloud structural similarity metric," in *IEEE International Conference on Multimedia Expo Workshops*, 2020, pp. 1–6.
- [18] D. Tian and G. AlRegib, "Batex3: Bit allocation for progressive transmission of textured 3-d models," *IEEE Transactions on Circuits and Systems for Video Technology*, vol. 18, no. 1, pp. 23–35, 2008.
- [19] J. Guo, V. Vidal, I. Cheng, A. Basu, A. Baskurt, and G. Lavoue, "Subjective and objective visual quality assessment of textured 3d meshes," *ACM Transactions on Applied Perception (TAP)*, vol. 14, no. 2, 2016.
- [20] G. Meynet, Y. Nehmé, J. Digne, and G. Lavoué, "Pcqm: A full-reference quality metric for colored 3d point clouds," in *International Conference on Quality of Multimedia Experience*, 2020, pp. 1–6.
- [21] Q. Liu, H. Yuan, R. Hamzaoui, H. Su, J. Hou, and H. Yang, "Reduced reference perceptual quality model with application to rate control for video-based point cloud compression," *IEEE Transactions on Image Processing*, vol. 30, pp. 6623–6636, 2021.
- [22] E. Alexiou and T. Ebrahimi, "Towards a point cloud structural similarity metric," in *2020 IEEE International Conference on Multimedia & Expo Workshops (ICMEW)*. IEEE, 2020, pp. 1–6.
- [23] Q. Yang, Z. Ma, Y. Xu, Z. Li, and J. Sun, "Inferring point cloud quality via graph similarity," *IEEE Transactions on Pattern Analysis and Machine Intelligence*, 2020.
- [24] G. Meynet, Y. Nehmé, J. Digne, and G. Lavoué, "Pcqm: A full-reference quality metric for colored 3d point clouds," in *2020 Twelfth International Conference on Quality of Multimedia Experience (QoMEX)*. IEEE, 2020, pp. 1–6.
- [25] Z. Zhang, W. Sun, X. Min, T. Wang, W. Lu, W. Zhu, and G. Zhai, "A no-reference visual quality metric for 3d color meshes," in *2021 IEEE International Conference on Multimedia & Expo Workshops (ICMEW)*. IEEE, 2021, pp. 1–6.
- [26] Z. Zhang, W. Sun, X. Min, T. Wang, W. Lu, and G. Zhai, "No-reference quality assessment for 3d colored point cloud and mesh models," *IEEE Transactions on Circuits and Systems for Video Technology*, 2022.
- [27] Q. Yang, H. Chen, Z. Ma, Y. Xu, R. Tang, and J. Sun, "Predicting the perceptual quality of point cloud: A 3d-to-2d projection-based exploration," *IEEE Transactions on Multimedia*, pp. 1–1, 2020.
- [28] E. M. Torlig, E. Alexiou, T. A. Fonseca, R. L. de Queiroz, and T. Ebrahimi, "A novel methodology for quality assessment of voxelized point clouds," in *Applications of Digital Image Processing XLI*, vol. 10752. International Society for Optics and Photonics, 2018, pp. 174–190.
- [29] Q. Liu, H. Yuan, H. Su, H. Liu, Y. Wang, H. Yang, and J. Hou, "Pqa-net: Deep no reference point cloud quality assessment via multi-view projection," *IEEE Transactions on Circuits and Systems for Video Technology*, 2021.
- [30] B. Li, W. Zhang, M. Tian, G. Zhai, and X. Wang, "Blindly assess quality of in-the-wild videos via quality-aware pre-training and motion perception," *IEEE Transactions on Circuits and Systems for Video Technology*, 2022.
- [31] W. Sun, X. Min, W. Lu, and G. Zhai, "A deep learning based no-reference quality assessment model for ugc videos," *arXiv preprint arXiv:2204.14047*, 2022.
- [32] Q. Liu, H. Su, Z. Duanmu, W. Liu, and Z. Wang, "Perceptual quality assessment of colored 3d point clouds," *IEEE Transactions on Visualization and Computer Graphics*, 2022.
- [33] Y. Liu, Q. Yang, Y. Xu, and L. Yang, "Point cloud quality assessment: Dataset construction and learning-based no-reference metric," *ACM Transactions on Multimedia Computing, Communications, and Applications (TOMM)*, 2022.
- [34] —, "Point cloud quality assessment: Large-scale dataset construction and learning-based no-reference approach," *arXiv preprint arXiv:2012.11895*, 2020.
- [35] Z. Wang, A. Bovik, H. Sheikh, and E. Simoncelli, "Image quality assessment: from error visibility to structural similarity," *IEEE Transactions on Image Processing*, vol. 13, no. 4, pp. 600–612, 2004.
- [36] "Vmaf - video multi-method assessment fusion," May. 30, 2022. [Online]. Available: <https://github.com/Netflix/vmaf>
- [37] A. Mittal, R. Soundararajan, and A. C. Bovik, "Making a "completely blind" image quality analyzer," *IEEE Signal Processing Letters*, vol. 20, no. 3, pp. 209–212, 2013.
- [38] A. Mittal, M. A. Saad, and A. C. Bovik, "A completely blind video integrity oracle," *IEEE Transactions on Image Processing*, vol. 25, no. 1, pp. 289–300, 2015.
- [39] M. A. Saad, A. C. Bovik, and C. Charrier, "Blind prediction of natural video quality," *IEEE Transactions on Image Processing*, vol. 23, no. 3, pp. 1352–1365, 2014.
- [40] J. Korhonen, "Two-level approach for no-reference consumer video quality assessment," *IEEE Transactions on Image Processing*, vol. 28, no. 12, pp. 5923–5938, 2019.
- [41] Z. Tu, Y. Wang, N. Birkbeck, B. Adsumilli, and A. C. Bovik, "Ugc-vqa: Benchmarking blind video quality assessment for user generated content," *IEEE Transactions on Image Processing*, vol. 30, pp. 4449–4464, 2021.
- [42] D. Li, T. Jiang, and M. Jiang, "Quality assessment of in-the-wild videos," in *Proceedings of the 27th ACM International Conference on Multimedia*, 2019, pp. 2351–2359.
- [43] Z. Tu, X. Yu, Y. Wang, N. Birkbeck, B. Adsumilli, and A. C. Bovik, "Rapique: Rapid and accurate video quality prediction of user generated content," *IEEE Open Journal of Signal Processing*, vol. 2, pp. 425–440, 2021.
- [44] W. Sun, T. Wang, X. Min, F. Yi, and G. Zhai, "Deep learning based full-reference and no-reference quality assessment models for compressed ugc videos," in *2021 IEEE International Conference on Multimedia & Expo Workshops (ICMEW)*. IEEE, 2021, pp. 1–6.
- [45] Q.-Y. Zhou, J. Park, and V. Koltun, "Open3D: A modern library for 3D data processing," *arXiv:1801.09847*, 2018.
- [46] Q. Yang, Z. Ma, Y. Xu, Z. Li, and J. Sun, "Inferring point cloud quality via graph similarity," *IEEE Transactions on Pattern Analysis and Machine Intelligence*, 2020.
- [47] I. Viola and P. Cesar, "A reduced reference metric for visual quality evaluation of point cloud contents," *IEEE Signal Processing Letters*, vol. 27, pp. 1660–1664, 2020.
- [48] A. Mittal, A. K. Moorthy, and A. C. Bovik, "No-reference image quality assessment in the spatial domain," *IEEE Transactions on Image Processing*, vol. 21, no. 12, pp. 4695–4708, 2012.
- [49] A. Chetouani, M. Quach, G. Valenzise, and F. Dufaux, "Deep learning-based quality assessment of 3d point clouds without reference," in *2021 IEEE International Conference on Multimedia & Expo Workshops (ICMEW)*, 2021, pp. 1–6.
- [50] Y. Fan, Z. Zhang, W. Sun, X. Min, W. Lu, T. Wang, N. Liu, and G. Zhai, "A no-reference quality assessment metric for point cloud based on captured video sequences," *arXiv preprint arXiv:2206.05054*, 2022.
- [51] K. He, X. Zhang, S. Ren, and J. Sun, "Deep residual learning for image recognition," in *Proceedings of the IEEE conference on computer vision and pattern recognition*, 2016, pp. 770–778.
- [52] C. Feichtenhofer, H. Fan, J. Malik, and K. He, "Slowfast networks for video recognition," in *Proceedings of the IEEE/CVF international conference on computer vision*, 2019, pp. 6202–6211.
- [53] J. Deng, W. Dong, R. Socher, L.-J. Li, K. Li, and L. Fei-Fei, "Imagenet: A large-scale hierarchical image database," in *2009 IEEE conference on computer vision and pattern recognition*. Ieee, 2009, pp. 248–255.
- [54] W. Kay, J. Carreira, K. Simonyan, B. Zhang, C. Hillier, S. Vijayanarasimhan, F. Viola, T. Green, T. Back, P. Natsev *et al.*, "The kinetics human action video dataset," *arXiv preprint arXiv:1705.06950*, 2017.
- [55] D. P. Kingma and J. Ba, "Adam: A method for stochastic optimization," *arXiv preprint arXiv:1412.6980*, 2014.
- [56] V. Hosu, F. Hahn, M. Jenadeleh, H. Lin, H. Men, T. Szirányi, S. Li, and D. Saupé, "The konstanz natural video database (konvid-1k)," in *2017 Ninth international conference on quality of multimedia experience (QoMEX)*. IEEE, 2017, pp. 1–6.
- [57] V. Hosu, H. Lin, T. Sziranyi, and D. Saupé, "Koniq-10k: An ecologically valid database for deep learning of blind image quality assessment," *IEEE Transactions on Image Processing*, vol. 29, pp. 4041–4056, 2020.
- [58] K. Simonyan and A. Zisserman, "Very deep convolutional networks for large-scale image recognition," *arXiv preprint arXiv:1409.1556*, 2014.
- [59] M. Sandler, A. Howard, M. Zhu, A. Zhmoginov, and L.-C. Chen, "Mobilenetv2: Inverted residuals and linear bottlenecks," in *Proceedings of the IEEE conference on computer vision and pattern recognition*, 2018, pp. 4510–4520.
- [60] C. Feichtenhofer, "X3d: Expanding architectures for efficient video recognition," in *Proceedings of the IEEE/CVF Conference on Computer Vision and Pattern Recognition*, 2020, pp. 203–213.
- [61] H. Sheikh, M. Sabir, and A. Bovik, "A statistical evaluation of recent full reference image quality assessment algorithms," *IEEE Transactions on Image Processing*, vol. 15, no. 11, pp. 3440–3451, 2006.